10th CIRP Global Web Conference – Material Aspects of Manufacturing Processes

FEM-based simulation of continuous wear of CrAlN-coated tools

Bernd Breidenstein[a]*, Benjamin Bergmann[a], Sascha Beblein[b], Florian Grzeschik[a]

[a] *Institute of Production Engineering and Machine Tools (IFW), Leibniz Universität Hannover, An der Universität 2, 30823 Garbsen, Germany*
[b] *LMT Tools GmbH & Co. KG, Grabauer Str. 24, 21493 Schwarzenbek, Germany; Sascha.Beblein@LMT-Group.net*

* Corresponding author. Tel.: +49-511-762-5206; fax: +49-511-762-5115. E-mail address: breidenstein@ifw.uni-hannover.de

Abstract

The understanding of the correlation between the coating-specific properties of PVD-coated cutting tools, the thermomechanical loads on the cutting wedge and the resulting tool wear, is necessary to avoid costly iterative test series. To obtain this knowledge a hybrid approach based on experimental tests and FEM-based chip formation is used in this study. In this respect, in a first step, a suitable wear rate model is derived and parameterized on the basis of wear analogy tests and experimental machining investigations. This wear rate model is then coupled with the FEM-based chip formation simulation to predict continuous tool wear.

Keywords: PVD-Coating, Cutting, FE-Simulation, Tool wear

1. Introduction

Cemented carbide currently accounts for the largest share of the cutting materials available and used on the market, at approximately 60 % of a total market volume of 17 billion US dollars (extrapolated from [1]). An established approach to reduce the wear of cemented carbide tools is the use of coatings, which have been state of the art in the field of machining since their introduction in 1970. The market share of coated cemented carbide tools is subject to a continuous increase compared to uncoated tools. Today, approximately 94 % of all cemented carbide tools used worldwide are coated (extrapolated from [1]).

Due to knowledge deficits regarding the cause-and-effect relationship between the coating parameters and the resulting coating properties, a large number of iterative parameter studies characterizes coating development today. In addition, machining tests to evaluate the performance of the coatings are associated with high costs, time and resources. A major obstacle for the systematic design of application-specific

coating systems is the lack of knowledge about the influence of the coating properties on the resulting tool wear. One approach to reduce the number of experimental investigations and to generate a deeper understanding of the interactions between the coating properties, the thermomechanical load spectrum and the resulting wear is the application of chip formation simulations. A frequently used method to predict tool wear is based on the coupling of Finite Element (FE) based chip formation simulations with mathematical wear rate models. The latter describes the material loss per time unit as a function of the acting load spectrum. So far, models have been developed to describe individual wear mechanisms such as abrasion [2, 3], adhesion [4] and diffusion [5] as well as combined mechanisms [6, 7]. In contrast to empirical and analytical models, which are often based on simplifications and assumptions, the FE-based chip formation simulation allows the calculation of the input variables of the wear rate models (e.g. temperatures, stresses and relative sliding velocity between tool and chip) with high temporal and spatial resolution. A major disadvantage of chip formation simulations is the high calculation effort and the

associated long calculation times despite technical progress and increasing computing capacities. With this background, Yen et al. [8] developed a novel method in which the wear progress was divided into discrete time intervals. The tool load was determined by means of chip formation simulation for a defined wear condition of the tool and assumed to be constant over a defined time step for calculating the wear related change of the tool geometry based on Usui's wear model [4]. In order to calculate longer process times, this simulation cycle was repeated until a defined stopping criterion was reached. Utilizing this procedure, both the flank and the rake face wear could be calculated in good agreement with experimental investigations. In subsequent work, the approach proposed by Yen et al. was adopted by several authors to simulate tool wear using different cutting material and workpiece combinations. Outeiro et al. [9] used this methodology to simulate the wear of PcBN tools during hard machining of X40CrMoV5-1 (55 HRC). Schulze and Zanger [10] developed a 2D model to calculate the tool wear of uncoated carbide tools during the machining of the titanium alloy Ti-6Al-4V, taking into account the cyclically changing tool load due to segmented chip formation. The transfer of the described methodology to the three-dimensional calculation of tool wear was first performed by Attanasio et al. [11] for external longitudinal turning of C45 with uncoated carbide tools. Here, the wear model of Takeyama and Murata [6] was used to determine the abrasive and diffusive tool wear. Binder et al. [12, 13] developed a simulation model which for the first time considers the wear of TiAlN-coated cemented carbide tools during the external longitudinal turning of C45 in a 3D model. The authors used a modified wear model according to Usui, in which the normal stress σ_n was replaced by the maximum tangential stress τ_{max} [12]. In a previous study by Bergmann [14], a 2D model was developed by parameterizing the Usui wear model with the help of which external tool loads of uncoated carbide tools with different cutting edge roundings could be calculated during orthogonal turning. These loads are used to determine both the resulting wear and the optimum cutting edge rounding.

The main obstacle of the currently established wear rate models is that the relevant coating properties are not or not completely integrated. Thus, a variation of the coating system requires a redetermination of the material-specific parameters. In order to circumvent this and thus avoid the additional experimental and simulative effort, existing wear rate models are to be extended by the influence of specific layer properties.

2. Experimental setup

2.1. Oxidation tests

In order to determine the substrate- and coating-specific oxidation behaviour, both uncoated and coated ($Cr_{1-x}Al_xN$-based coatings) cemented carbide samples (type Ceratizit CTS 12D) are subjected to an isothermal annealing test in an air atmosphere. A Nabertherm N21 chamber furnace is used for this purpose. The thermal boundary conditions are varied as described in Table 1. Due to the significantly greater tendency of the uncoated tools to oxidize, they were tested at lower temperatures.

Table 1: Parameters of the oxidation tests

Annealing temperature T (uncoated)	Annealing temperature T (coated)	Holding time t_H
[°C]	[°C]	[h]
500	800	1
700	900	2
900	1.000	3

2.2. Experimental cutting tests and coating deposition

The experimental cutting tests were carried out on a Gildemeister CTV400 CNC vertical lathe in orthogonal cut without coolant. Tubes of AISI4140 with a diameter of 100 mm and a wall thickness of 3 mm were machined. The cutting speed was set to $v_c = 150$ m/min and the uncut chip thickness to $h = 0.1$ mm. The wedge angle of the tools is $\beta = 90°$. A clearance angle of $\alpha = 6°$ was set, resulting in an effective rake angle of $\gamma = -6°$ taking the wedge angle into account. WC-Co cemented carbide tools of the geometry SNUN120408 were used in the investigations. In order to ensure sufficient adhesion of the coating, the substrates were subjected to extensive pretreatment. This included microblasting, wet chemical cleaning and plasma etching.

$Cr_{1-x}Al_xN$-based nitride coatings were deposited by reactive magnetron sputtering on cemented carbide inserts using an industrial PVD magnetron sputter unit of type Cemecon CC800/9. Subsequently, these coatings were undergoing a fundamental characterization with regard to the chemical, structural and mechanical-technological coating properties. The coatings chemical composition was varied by variable target configuration using segmented targets of chromium (20 – 70 %) and aluminium (30 – 70 %) segments. In order to obtain variable mechanical properties and coating thicknesses, bias voltage (110 - 135 V), coating duration (0.5 - 2.1 h), coating mode (HiPIMS, DCMS/HiPIMS), target power (5 - 7 kW) and $Ar/-N_2$-ratio (1.5 - 5.1) were varied.

The indentation hardness H_{IT} and the indentation modulus E_{IT} of the coatings were obtained according to EN ISO 14577-1 from indentation load-displacement data. As already described in [15], a high positive correlation between those properties was found. The tests are carried out with a UNAT tester from ASMEC, with a maximum penetration depth of 10% of the coating thickness. The coating thickness was determined by means of scanning electron microscopy (SEM) of cross-sections of the coated inserts. A homogeneous coating thickness distribution along the cutting edge profile was

observed in all samples. In order to determine an average coating thickness, three measurements were carried out on the rake face, cutting edge rounding and flank face. For the chemical analysis of the layer composition, a Glow Discharge Optical Emission Spectroscopy (GDOES) was performed with a spectroscope of the type GDA 750 from the company Spektruma Analytik.

The cutting edge microgeometry was determined using the optical measurement system Alicona Infinite Focus G5. A mean cutting edge section S = 50 ± 5 μm was determined for all cutting tools. A Keyence VHX-600 digital microscope was used to measure the width of the flank wear land VB_{max}. For detailed investigations of the wear behaviour, SEM analyses and EDX measurements were additionally carried out for selected tools.

2.3. Simulation model

Two-dimensional chip formation simulations were carried out using Deform-2D v11.2. The simulation approximates the turning process as a two-dimensional orthogonal cut in the wedge measuring plane assuming plain strain conditions and a three-dimensional stress state. The calculation is based on the implicit Lagrangian formulation with automatic remeshing. The modelling of the plastomechanical flow behaviour of the material, characterised by the flow stress σ_f, is based on the phenomenological material model according to Johnson and Cook as a function of strain, strain rate and temperature. Furthermore, temperature dependent thermomechanical material properties of AISI 4140 are used. The required data were taken from the Deform database. The tool is assumed to be ideally rigid. A detailed description of the substrate properties is given in [15]. The modeling of the friction behaviour is based on the hybrid approach proposed by Zorev [16]. Assuming that the maximum tangential stress on the tool is physically limited by the shear flow stress of the plastically deformed material, the friction factor was defined as m = 1. In addition, a coefficient of friction μ = f(v_g) was applied based on the findings in [17]. A value of h = 100 kW/m²K was used for the heat transfer coefficient. In order to represent larger cutting paths, a multilevel discrete-time approach for the simulation of tool wear is used, as described in [14], following [8].

3. Experimental results

3.1. Wear investigations

For the selection, parameterization and validation of the wear rate model, the mechanisms of action of the coating wear must be understood, taking into account the coating properties. For this purpose, the wear-related change of the microgeometry at different operating times was recorded intermittently during machining investigations in orthogonal plane turning. In a further step, these findings were used to calculate the local wear rates along the contact zone. The wear investigations are carried out at constant process parameters (v_c = 150 m/min h = 0.1 mm, b = 3 mm) up to a maximum width of the flank wear land of VB_{Bmax} = 150 μm. By varying the chromium

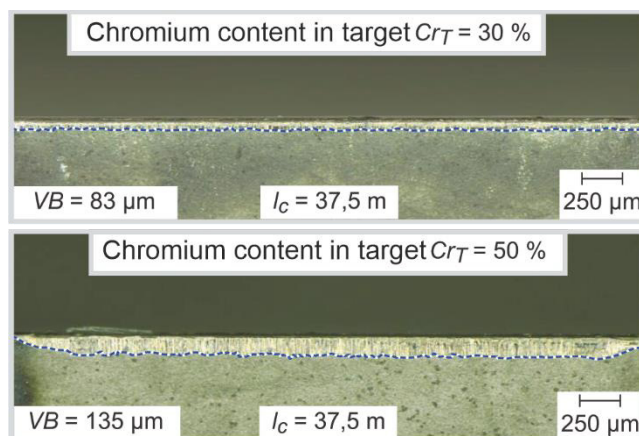content in the target, the wear behavior can be significantly influenced (Fig. 1).

Fig. 1. Influence of chromium content on flank face wear.

The increase in chromium content in the target is accompanied by a reduction in wear resistance despite increasing hardness. Thus, the increase of the chromium content by 20 % leads to an increase of the width of the flank wear land by more than 50 %. In addition, EDX analysis confirmed material adhesion and adhesion as the dominant wear mechanism. Above 50 % chromium content in the target, there is a drastic decrease in tool life (Fig. 2).
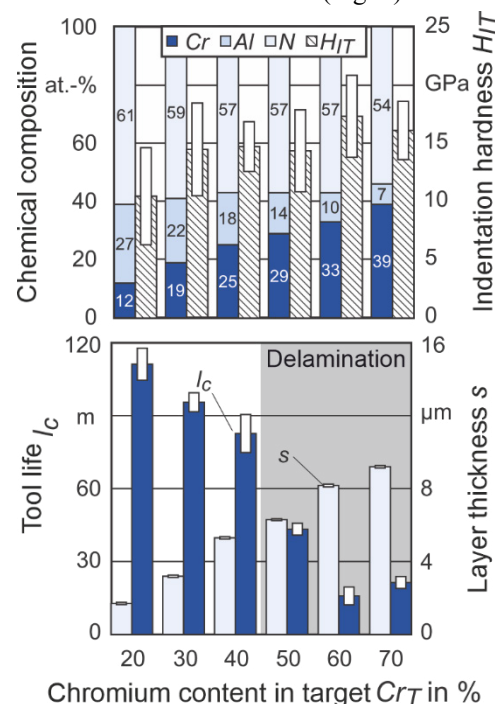

Fig. 2. Influence of the chromium content in the target on coating properties and tool life.

This can be explained by the resulting coating thicknesses of s > 5 μm. This leads to increased adhesive layer failure, which can even lead to delamination in the area of the microgeometries of the cutting edges. Furthermore, the figure shows that increasing the chromium content in the target from 20 % to 70 % leads to an increase in the chromium content

from 12 % to 39 % in the layer. Due to the increased chromium content, the proportion of metallic bonds in the layer increases, which leads to increased adhesive behavior to the test material AISI 4140.

3.1. Oxidation tests

In the oxidation tests, as expected, a lower oxidation resistance was observed for the uncoated compared to the coated samples. As shown in figure 3, this is represented by the increase in mass per unit area Δm, which occurs as a result of the oxidation processes. Furthermore, a significant influence on the oxidation behavior was observed when varying the chemical composition of the coating.
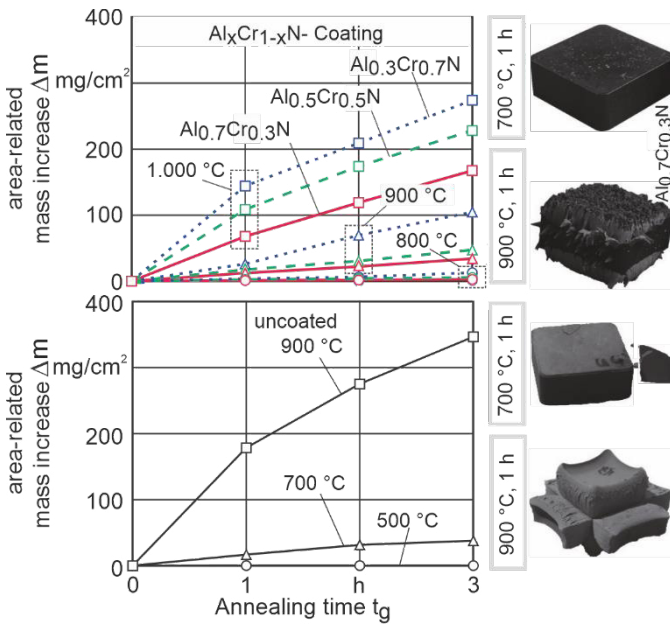

Fig. 3. Oxidation behavior of substrate and coating under variation of chemical layer composition.

The oxidation resistance decreases significantly with increasing chromium content in the coating. In order to be able to use these findings for wear simulation, knowledge of the activation energy E_A is necessary. This can be related to the reaction rate k_{Arr}, the temperature T and the universal gas constant R using Arrhenius' approach (equation 1). The factor k_0 represents the mathematical limit value for unrealizable temperatures (T→ ∞).

$$k_{Arr} = k_0 \cdot e^{\left(\frac{-E_A}{R \cdot T}\right)} \tag{1}$$

In order to be able to infer the activation energy from this approach, the surface-related mass increase per unit time is plotted logarithmically against the inverse of the temperature (Fig. 4). From the resulting linear behavior, a line equation can be formulated for the Arrhenius approach. From this, the activation energy can be calculated from the slope of the line, multiplied by the universal gas constant R. According to the previously presented results, the uncoated samples exhibit the lowest activation energies. Whereas the activation energies of the coatings increase with increasing aluminium content.
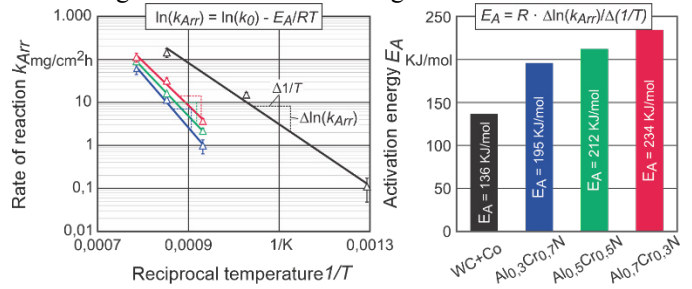

Fig. 4. Determination of the layer- and substrate-specific activation energy.

4. Parameterization of the wear rate model

The following parameterization is based on the one hand on the experimental results presented in section 3 and on the other hand on the results of the previous paper by Bergmann [14]. For this purpose, only cutting edge microgeometries and coating variants were used which exhibited continuous wear. Initially, the parameterization of the wear rate model according to Usui (equation 2) is carried out for the uncoated carbide tools. For this purpose, the corresponding wear rates are first determined for different wear states x and cutting edge microgeometries (cutting edge section on the flank face S_α and cutting edge section on the rake face S_γ). At the same time, temperatures, stresses and relative velocities are determined with the aid of the FEM-simulation, which are presented in the results of Bergmann [14]. The choice of the wear model is based on the dominant adhesive behavior of the tools.

$$\frac{dW}{dt} = C_1 \cdot \sigma_n \cdot v_g \cdot e^{\left(\frac{-C_2}{T}\right)} \tag{2}$$

Usui describes the wear rate as a function of the normal stress σ_n, the sliding speed v_g, the rake face temperature T and the material-specific constants C_1 and C_2. Logarithmizing this model yields equation 3, which in turn can be transformed into equation 4.

$$\ln\left(\frac{dW}{dt}\right) = \ln(C_1) + \ln(\sigma_n) + \ln(v_g) - \left(\frac{C_2}{T}\right) \tag{3}$$

$$\ln\left(\frac{dW}{dt \cdot \sigma_n \cdot v_g}\right) = \ln(C_1) - C_2\left(\frac{1}{T}\right) \tag{4}$$

By logarithmically plotting the wear rate against the inverse of the temperature, a linear relationship is obtained between these results (Fig. 5). Thus, the material-specific constants C_1 and C_2 can be determined as the intersection of the straight line with the abscissa (C_1) and as the slope of the straight line (C_2).

In common wear rate models, such as those according to Usui, the parameter sets determined in this way are material-specific and have been developed for cemented carbids. As a result, they can only be transferred to coatings with different compositions to a limited extent and are subject to calculation errors. The wear rate models set up so far lack the fact that relevant layer properties are not completely integrated. This means that the parameter sets have to be redefined when the

layer variation is changed, which can be avoided by integrating specific layer properties into existing wear rate models.
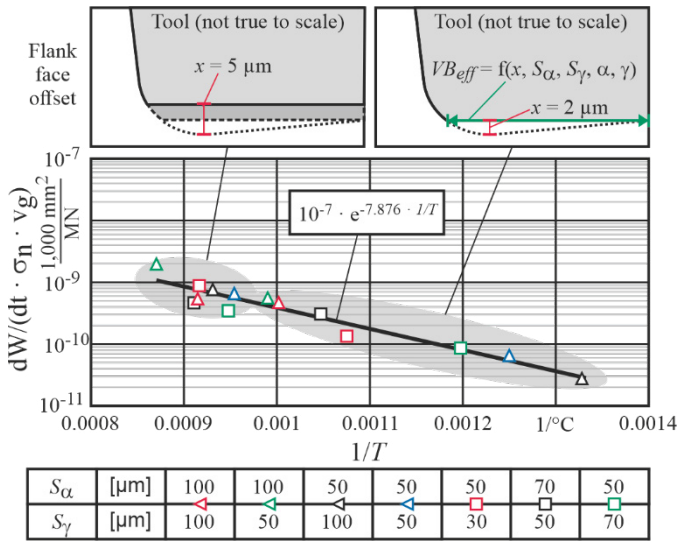

Fig. 5. Parameterization of the wear rate model according to Usui for uncoated carbide tools.

In order to transfer this wear rate model to coated tools, the relevant coating properties must be integrated. The material-specific parameter C_1 can be described in simplified terms as adhesion tendency due to the experimentally proven strong adhesive wear. This can be reduced by increasing the AlN/CrN ratio, which can be traced back to the increase in the covalent bond proportions in the coating. In order to determine the relationship between the parameter C_1 and the AlN/CrN ratio, the wear rate model was parameterized for different coating variants and the constant C_1 was extracted. Subsequently, a regression between the parameter C_1 and the AlN/CrN ratio was set up (Fig. 6).
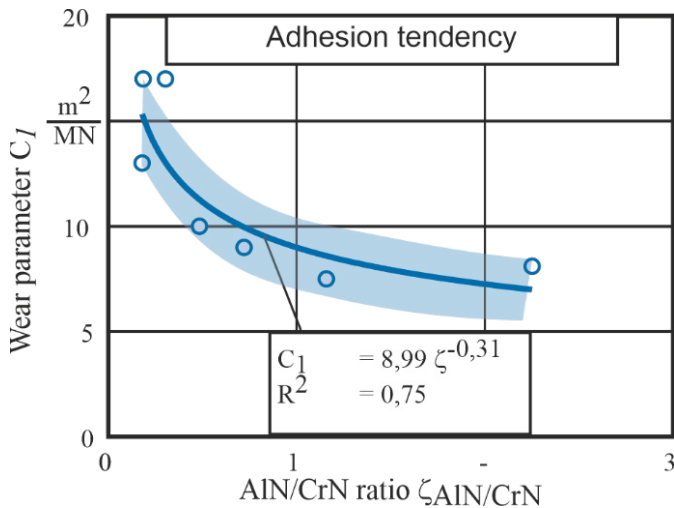

Fig. 6. Influence of the AlN/CrN ratio on the adhesive wear coefficient according to Usui.
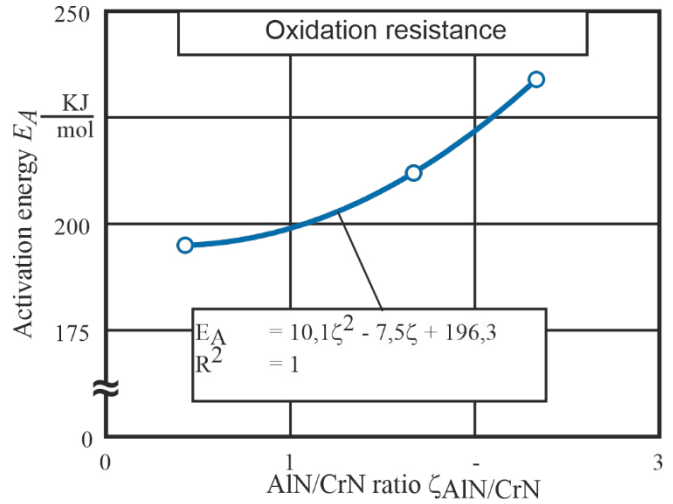

Fig. 7. Influence of the AlN/CrN ratio on the activation energy according to Usui.

The parameter C_2 in the wear model according to Usui can be described via the sensitivity to physicochemical wear, such as oxidation. The annealing tests showed that an increase in the AlN/CrN ratio is accompanied by increased oxidation resistance, which can be described by the activation energy. Therefore, to extend the wear rate model, in the following the parameter C_2 is described by the ratio of activation energy and universal gas constant (Fig. 7).

From the previously presented data, the wear rate model extended by the layer-specific wear resistance can be set up (equation 5). For this purpose, both the adhesive wear resistance C_1 and the activation energy are made to depend on the AlN/CrN ratio ζ.

$$\frac{dW}{dt} = C_1(\zeta) \cdot \sigma_n \cdot v_g \cdot e^{\left(\frac{-E_A(\zeta)}{R \cdot T}\right)} \tag{5}$$

5. Validation of the simulation

In order to map cutting paths necessary for wear simulation, a multilevel discrete-time approach was used as described in Bergmann [14] (Fig. 8). For this purpose, a chip formation simulation is first carried out with an unworn tool until a quasi-stationary state is reached. The load variables determined in this state are used as input variables for the calculation of the tool wear for this time step. In a further step, the remeshing of the FE mesh is calculated from this wear. The new tool geometry generated in this way can then be used as an input variable in the next chip formation simulation.

In order to validate the wear model, the wear curves of six different coating variants were used in figure 9 and the simulated curves were compared with the experimentally measured results.
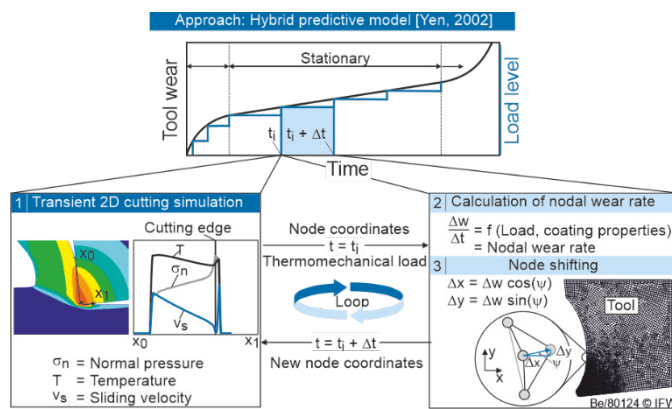
Fig. 8. Calculation cycle for the simulation of continuous layer wear [14].

By this, the simulated and experimentally determined wear curves show a qualitatively good agreement. Only at higher AlN/CrN ratios (samples 5 and 6) higher deviations tend to occur at the start of the process.
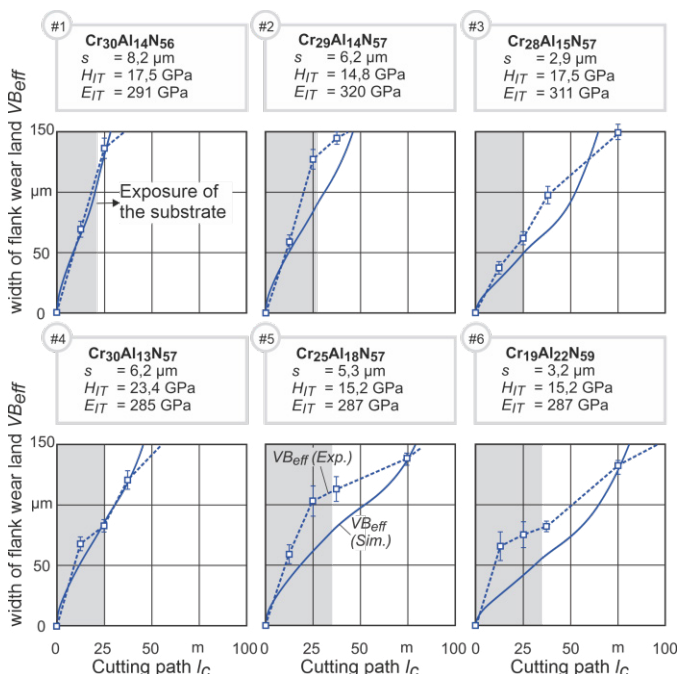

Fig. 9. Validation of the wear simulation.

6. Conclusion

The state of the art and the results of this work show that the performance of cutting tools can be significantly influenced by adapting the coating properties to the workpiece material and the cutting process. In addition to the coating, the tool load is also influenced by various geometric aspects such as the micro- and macrogeometry of the cutting tool as well as the substrate and the process parameters.

Therefore, for a load adapted coating design it is necessary to consider the properties and boundary conditions of the entire system. A major obstacle to the systematic and targeted design of application-specific coating systems is the lack of knowledge about the influence of coating properties in interaction with other system properties on the resulting tool wear. A purely simulative solution approach is not feasible due to the long calculation time, which is why a hybrid approach for determining the local load collectives and calculating the tool wear is necessary. Likewise, such a hybrid approach is able to exclude possible inaccuracies in the material model and the effects on the calibratability of the wear model parameters.

Acknowledgments

References

[1] Bobzin K. High-performance coatings for cutting tools. CIRP Journal of Manufacturing Science and Technology 2017; p. 1 – 9.
[2] Archard J. F. Contact and rubbing of flat surfaces. Journal of applied physics 1953; p. 981 – 988.
[3] Rabinowicz E, Dunn L, Russell P. A study of abrasive wear under three body conditions. Wear 4 1961; p. 345-35.
[4] Usui E, Shirakashi T, Kitagawa T. Analytical prediction of cutting tool wear. Wear Vol 100 1984; p. 129 – 151.
[5] Molinari A, Nouari M. Modeling of tool wear by diffusion in metal cutting. Wear 252 2002; p. 135 – 149.
[6] Takeyama H, Murata T. Basic investigation of tool wear. ASME Journal of engineering for industry 1963; p. 33 – 37.
[7] Huang Y, Dawson T. Tool Crater wear depth modeling in CBN hard turning. Wear 2005; p. 1455 – 1461.
[8] Yen Y, Söhner J, Weule H, Schmidt J, Altan T. Estimation of tool wear of carbide tool in orthogonal cutting using the FEM simulation. International journal of machining science and technology 2002; p. 467 – 486.
[9] Outeiro J, Umbrello D, Pina J, Rizzuti S. Modelling of tool wear and residual stress during machining of AISI H13 tool steel. Materials Processing and Design: Modeling, Simulation and Applications. Proceedings of the 9th International Conference on Numerical Methods in Industrial Forming Processes, AIP Conference Proceedings 2007; p. 1155 – 1160.
[10] Schulze V, Zanger F. Development of a simulation model to Investigate tool wear in Ti-6Al-4V alloy machining. Advanced Materials Research 2011; p. 535 – 544.
[11] Attanasio A, Ceretti E, Rizzuti S, Umbrello D, Micari F. 3D finite element analysis of tool wear in machining. CIRP Annals - Manufacturing Technology 2008; p. 63 – 64.
[12] Binder M, Klocke F, Lung D. Tool wear simulation of complex shaped coated cutting tools. Wear 2015; p. 600 – 607.
[13] Binder M, Klocke F, Doebbeler B. An advanced numerical approach on tool wear simulation for tool and process design in metal cutting. Simulation modelling practice and theory 2017; p. 65 – 82.
[14] Bergmann B, Denkena B, Beblein S, Picker T. E-Simulation Based Design of Wear-Optimized Cutting Edge Roundings. Journal of Manufacturing and Materials Processing 5, 2021.
[15] Beblein S, Breidenstein B, Denkena B, Pusch C, Hoche H, Oechsner M. Thermomechanical Coating Load in Dependence of Fundamental Coating Properties. Procedia CIRP 2017; p. 25 – 30.
[16] Zorev N. Inter-relationship between shear processes occurring along the tool face and shear plane in metal cutting. International Research in Production Engineering ASME 1963; p. 42 – 49.
[17] Denkena B, Krödel A, Beblein S. A novel approach to determine the velocity dependency of the friction behavior during machining by means of digital particle image velocimetry (DPIV). CIRP Journal of Manufacturing Science and Technology 2021; p. 81-90.